Modelling of a flap type wave energy converter farm in a mild-slope equation model for a wake effect assessment

Nicolas Tomey-Bozo[1,*], Jimmy Murphy[1], Peter Troch[2], Tony Lewis[1], Gareth Thomas[3]

[1]Centre for Marine and Renewable Energy (MaREI), ERI - Beaufort Building, University College Cork, Haulbowline Road, Ringaskiddy, Co. Cork, Ireland
[2]Ghent University, Department of Civil Engineering, Technologiepark 904, B-9052 Zwijnaarde, Belgium
[3]School of Mathematical Sciences, 145 Western Gateway Building, University College Cork, Cork, Ireland
[*]nicolas.tomey@ucc.ie

Abstract: It is expected that large farms of Wave Energy Converters (WECs) will be installed and as part of the consenting process it will be necessary to quantify their impact on the local environment. The objective of this study is to assess the impact a WEC farm has on the incoming wave field through the use of a novel methodology. This methodology assesses the changes of the significant wave height surrounding a flap type WEC farm with a special focus on the lee of the farm. A time-dependent mild-slope equation model is employed to solve the propagation of surface waves and their interaction with the devices. The model represents the devices as obstacle cells with attributed absorption coefficients tuned against near-fields obtained from a Boundary Element Method (BEM) solver. The wake effect of the farm is determined by using a step by step approach starting first with an assessment of one device and progressively incrementing to a larger number of flaps. The effect of incident sea states, device separations, and water depth changes on the wake effect of the farm are also investigated. This work shows the potential of a WEC farm to reduce significant wave heights on the leeside.

1. Introduction

Wave energy converters (WECs) transform the incoming waves from the ocean by partially absorbing and partially redistributing the wave energy arriving to the device. Part of the energy is extracted and transformed into electricity while another part is redistributed by a combination of diffraction and radiation phenomena into the ocean. The transformation of the incoming wave energy then leads to a reduction of the wave energy density in the lee of the device. The amount of energy reduction increases with the number of devices allowing for of a large sheltered zone to be created in the lee of the WEC farm. This sheltered zone can be profitable for other marine activities that would benefit from a reduction of the wave energy density in a delimited area. Examples of these activities are offshore wind farms, aquaculture fisheries, or coastal protection projects.

The modelling of WECs to quantify their impact on the wave climate is still a relatively new area of study. Different methodologies have been implemented to attempt to quantify the wave field surrounding a WEC farm but up to date there is not an ideal ready-to-use tool to assess this problem. Boundary Element Method (BEM) solvers based on potential flow have been used to

assess the near field effects and farm interactions [1, 2] because of their high suitability to solve wave-body interaction problems. However, BEM solvers present some limitations due to their constant water depths assumption and therefore the absence of wave transformation processes. Wave propagation models, using either phase averaged [3, 4] or phase-resolved models [5, 6], have been applied to study the far field effects in large domains. These models are accurate solvers of wave transformation processes across large domains and allow the consideration of realistic irregular bathymetries. Their main disadvantage remain the weak capacity of modelling moving bodies and the interaction with waves. An overview of the different methodologies with their advantages and disadvantages can be found in [11].

The most common applications of wave propagation models represent the devices as grid cells with attributed absorption coefficients or source terms. These absorption coefficients or source terms are tuned to match a look up table with reflection and transmission (and absorption inherently) coefficients used as a target to represent the effect of the WEC on the near field. Obtaining the correct target reflection and transmission coefficients is a difficult task as there is no clear procedure on the manner by which they are to be determined. Usually those transmission and reflection coefficients refer to the wave field information along a section line in the wave propagation direction which does not allow for the validation of the 2D wave field perturbation caused by the device. In addition, these coefficients are commonly obtained from tank testing where tank reflection remain an important issue, or from developer look up tables where the source of information remain uncertain due to the general unwillingness from developers to share it.

In this study a time-dependent mild-slope equation model (phase-resolved wave propagation model) is used to simulate the propagation of surface waves through a WEC farm. The target reflection and transmission effect of the WEC on the surrounding near-field is obtained from the wave field solutions calculated in a BEM solver. BEM solvers are regarded as being accurate in the local wave-body interaction problem as they account for all the wave components generated by a moving body [12]. The representation of the target wave reflection and transmission of the device as a complete wave field all around the device allows for the validation of the 2D wave field perturbation created by the presence of the WEC.

The device type selected is a flap type WEC located in shallow waters and subject to wave conditions consisting of irregular long crested waves. The tuning of the flap representation is achieved first by comparing near-field wave solutions from the BEM solver to the wave solutions from the mild-slope equation model. Then, the layout of the WEC farm is designed in an incremental manner by assessing the effect of, first a single flap, then a row of several flaps, and finally two rows of flaps, on the incoming wave field. The flaps are placed at the locations where the wave energy density is higher in order to achieve better energy absorption, thus resulting in a larger impact on the wave field. Finally, the sensitivity of the wake effect to the sea state, the device separation, and the bathymetry are also assessed. The model was setup with a large domain in order to evaluate the wake effect of a flap farm in the far-field and its potential sheltering effect.

2. Numerical tools

2.1. Open-source Boundary Element Method NEMOH

NEMOH is an open-source BEM solver developed by Ecole Centrale de Nantes [12] and it is used in this work to obtain the near-field surrounding the WECs. NEMOH is based on the linear potential theory and it calculates the perturbed velocity potential generated by the presence of a

floating body under an incoming regular wave. This is done by solving the scattering problem with the appropriate set of boundary conditions, which is the well-known linear wave body interaction boundary value problem. The velocity potential $\tilde{\phi}(x, y, z)$ for the perturbed wave is obtained as a 3D solution describing the flow surrounding the body. Then from the potential at the free surface condition $\tilde{\Phi}(x, y)$ where $z = 0$ it is straightforward to obtain the surface elevation $\tilde{\eta}$ as shown in Eqn. (1)

$$\tilde{\eta}(x, y) = \frac{i\omega}{g}\tilde{\Phi}(x, y) \tag{1}$$

where ω is the wave frequency and g the gravitational acceleration.

The scattering problem is solved for each wave frequency by dividing the problem into one diffraction problem and one radiation problem per degree of freedom of the moving body. The diffraction problem is computed considering the body is fixed under the presence of an incoming incident wave. The radiation problem is solved by considering a forced motion of the body in calm conditions (absence of waves). The sum of the surface elevation obtained from the diffraction problem and the radiation problems (one problem per degree of freedom) gives the surface elevation for the perturbed wave as shown in Eqn. (2). The solution of the total wave field (Eqn. (3)) is then obtained as a superposition of the surface elevation for the incident wave and the perturbed wave. Details of the equations solved by NEMOH to obtain the perturbed potential solution are described in detail in [12].

$$\tilde{\eta}_p(x, y) = \tilde{\eta}_d + \sum_{n=1}^{6} \tilde{\eta}_r \tag{2}$$

$$\tilde{\eta}_t(x, y) = \tilde{\eta}_i + \tilde{\eta}_p \tag{3}$$

Tilde ($\tilde{}$) denotes the complex form of the variables and subscripts p, d, r, t, and i refer to the perturbed, diffracted, radiated, total, and incident wave respectively. The complex surface elevation can be expressed as

$$\tilde{\eta} = A_\omega e^{i\varphi} \tag{4}$$

where the wave amplitude A_ω and phase φ are the module and argument.

2.2. Mild-slope equation model MILDwave

The core of the calculations carried out in this work are implemented using MILDwave, a time-dependent mild-slope equation model developed by Ghent University [14, 15]. MILDwave is a phase-resolved type wave propagation model that solves the propagation of surface waves throughout the domain and the interaction with the obstacles (previously defined) by solving the depth-integrated mild-slope equations of Radder and Dingemans [7]. The velocity potential and the instantaneous surface elevation at the free water surface are the variables solved for each coordinate of the grid (x,y) for each instant t of time by the set of differential equations given in equation (5) and (6):

$$\frac{\partial \eta}{\partial t} = B\Phi - \nabla(A\nabla\phi) \tag{5}$$

$$\frac{\partial \Phi}{\partial t} = -g\eta \tag{6}$$

where A and B are the coefficients described in Eqns. (7) and (8)

$$B = \frac{\bar{\omega}^2 - \bar{k}^2 \bar{C} \bar{C}_g}{g} \tag{7}$$

$$A = \frac{\bar{C} \bar{C}_g}{g} \tag{8}$$

with the phase velocity $\bar{C}$ and the group velocity $\bar{C}_g$ for a wave with carrier wave number $\bar{k}$ and carrier angular frequency $\bar{\omega}$. Overbar ($^-$) denotes that the wave characteristic is calculated for the carrier frequency.

Waves are generated in MILDwave at the offshore boundary by using the source term addition method, i.e. by adding an additional surface elevation η^* to the calculated value on a wave generation line for each time step given by equation (9) and described in [8]:

$$\eta^* = 2\eta_I \frac{C_e \Delta t}{\Delta x} \sin\theta \tag{9}$$

with the water surface elevation of incident waves η_I, the angle of wave rays from the Y axis θ, the grid size in X direction Δx, the time step Δt, and the energy velocity C_e given by equation (10):

$$C_e = \bar{C}_g \frac{\bar{\omega}}{\omega} \sqrt{1 + \frac{\bar{C}}{\bar{C}_g} \left(\left(\frac{\omega}{\bar{\omega}} \right)^2 - 1 \right)} \tag{10}$$

The wave generation line is assumed to be parallel to the Y axis in equation (9). For the generation of random waves, the peak frequency is used as a carrier frequency in equations (7) and (8) as the peak frequency is usually lower than the weight-averaged frequency and as the dispersion relation of the model of Radder and Dingemans is more accurate in the high frequency range [8, 9].

Obstacles are defined in MILDwave by grid cells that have attributed absorption coefficients. These absorption coefficients locally affect the surface elevation of the propagated wave which is multiplied by values in the range from 1 to 0. Values equal to 1 represent a water grid cell (no absorption) while values equal to 0 represent a grid cell of a fully reflective obstacle (100 % reflection). Therefore, the wave field reflection and transmission changes depending on the distribution of the absorption coefficients through the set of obstacles cells. Thus, wave energy converters can be represented as obstacle cells with absorption coefficients tuned to represent the target wave reflection and transmission (and absorption inherently).

3. Implementation of a wave energy converter in a mild-slope equation model

Wave propagation models are used in many engineering studies for determining site specific wave conditions. They can incorporate very large domains and realistic environmental conditions such as irregular bathymetries and shallow water wave transformation processes. However from a renewable energy perspective they do not accurately represent the local wave-body interaction problem when a moving body is considered. Nevertheless wave propagation models can still be the best option when the wake effect for a WEC farm in the far-field needs to be quantified. They can give a satisfactory balance between accuracy and computational time.

3.1. Overview of methodology

The solution suggested in this study to accurately model the WEC disturbance on the wave field is to tune the parameters representing the device in the wave propagation model against results obtained from BEM solvers for the near-field. BEM solvers give a complete solution of the local wave-body interaction problem by solving all wave components; the radiated wave generated by the motion of the device for each degree of freedom and the diffracted wave generated by the disturbance of the incident wave due to the presence of a fix body. Thus, whilst remaining under the limitations of the linear water theory, the solution obtained from a BEM solver is considered to be representative of the wave-body interaction phenomena for the near-field. The more the water depth changes with the distance to the device, the smaller is the near-field area surrounding the device where BEM solvers can provide accurate results.

Irregular long crested waves are considered in MILDwave to assess the wake effect generated by a WEC farm. Therefore, the same irregular sea state conditions need to be used as a target for the tuning of the absorption coefficients attributed to obstacle cells representing the device. First a superposition of the regular wave results obtained from NEMOH is computed to obtain the desired target irregular sea states. Then irregular long-crested waves are run in MILDwave and the obstacle cells representing the WEC are tuned against the target irregular wave solutions computed from NEMOH. Once the accurate configuration of absorption coefficients attributed to the obstacle cells is found, the wake effect of a farm with several devices can be assessed with the same obstacle cell configuration for each device. Finally, it is important to consider that each sea state has its own optimum configuration of obstacle cells and that a tuning of the device representation is needed for every case.

3.2. Flap type wave energy converter

The WEC considered in this study is a surface-piercing flap hinged at the bottom of the seabed as shown in Figure 1. The motion is restricted to pitch and therefore only one degree of freedom is considered. The shaft about which the flap rotates is at the base of the device.

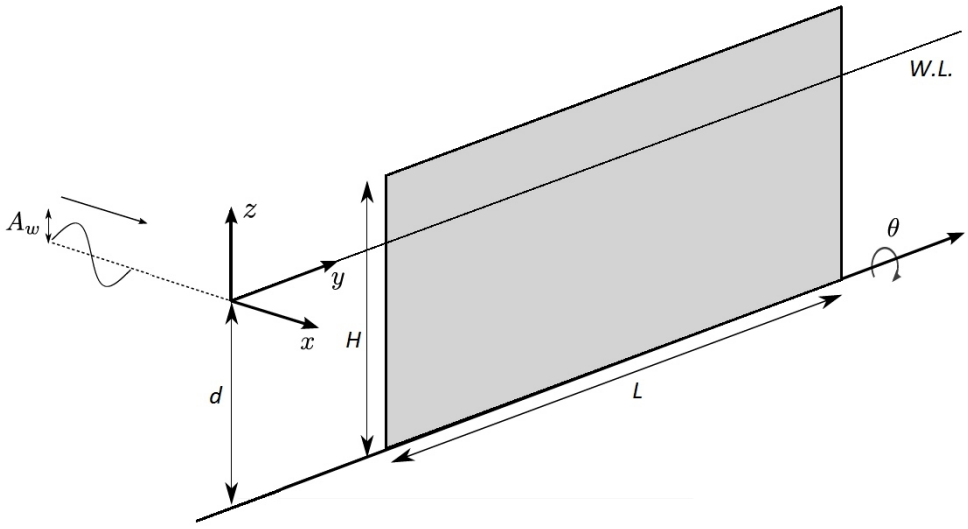

Fig. 1. *Flap type WEC sketch.*

The flap main characteristics are provided in Table 1 and the parameters θ, $W.L.$, and d represent the angle of pitch motion, the water line level, and the depth respectively.

Table 1 Main characteristics of the flap type WEC

Parameter	Symbol	Value	Units
Length	L	20	m
Height	H	12	m
Thickness	T	1	m
Relative density	ρ_r	0.3	-

The amplitude of the angle of motion is calculated based on equation (11). This value is used to quantify the radiated wave obtained from NEMOH which is non-dimensionalised by the amplitude of motion for the corresponding degree of freedom.

$$\Theta(\omega) = \frac{A_w \Gamma(\omega)}{-\omega^2(I + A_r) - i\omega(B_r + B_P TO) + H} \tag{11}$$

A_w represents the wave amplitude, Γ, the wave excitation moment coefficient, I, the moment of inertia about the Y axis, A_r, the added moment of inertia coefficient, B_r, the radiation damping coefficient, H, the hydrostatic restoring coefficient, and B_{PTO}, the Power Take Off (PTO) damping coefficient.

The optimum value of the PTO damping coefficient for each wave frequency is theoretically defined by equation (12) as demonstrated in [10]. As irregular sea states are applied in this study, the value of the PTO damping coefficient used is the optimum one for the frequency corresponding to the peak period of the sea state applied.

$$B_{PTO} = \sqrt{\left(\frac{H}{\omega} - \omega(I + A_r)\right)^2 + B_r^2} \tag{12}$$

3.3. Representation in NEMOH

As a first step the wave amplitude corresponding to the total wave solution is computed for each regular wave from the superposition of the perturbed wave obtained from NEMOH and its corresponding incident wave. A domain of 400 x 400 meters is considered as a representation of the near-field surrounding the device. Figure 2 shows the results obtained for an incident regular wave of $T = 8$ s and $A_\omega = 1$ m. The waves propagate towards the X positive axis for all cases considered for this study.

From the total wave amplitude obtained for regular waves it is possible to compute an irregular sea state which accounts for the perturbation of the WEC. This is done based on the superposition principle of linear water waves along a long range of frequencies representing a wave energy spectrum. The parameterised JONSWAP spectrum described in [5] is used to represent the wave spectral density distribution of the input incident long-crested irregular waves. A peak enhancement factor γ of 3.3 is considered and a discretisation of 100 wave frequency intervals is used.

The relation between the wave spectral density and the amplitude corresponding to each frequency interval is defined by equation (13):

$$S(\omega)\Delta\omega = \frac{1}{2} A_w(\omega)^2 \tag{13}$$

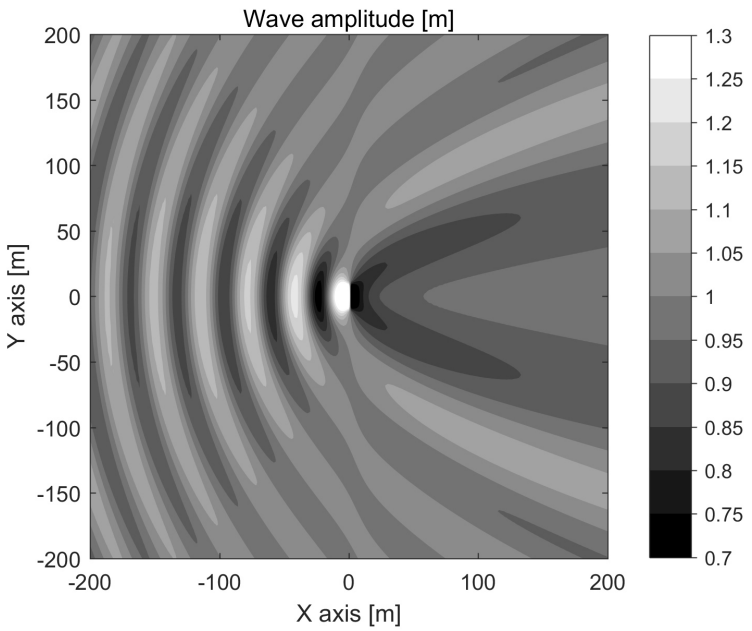

Fig. 2. *Total wave amplitude for a regular wave of* $T = 8$ *s and* $A_\omega = 1$ *m.*

where S is the wave spectral density and $\Delta\omega$ the increment between frequencies.

A disturbed wave spectrum is define now by equation (14) as the local transformation of the undisturbed wave spectrum caused by the presence of the WEC:

$$S_D(\omega) = S_U(\omega) A_{w_D}(\omega)^2 \tag{14}$$

where S_D is the disturbed wave spectrum, S_U the undisturbed spectrum, and A_{w_D} the disturbed wave amplitude obtained from the total wave amplitude results of each regular wave. Therefore, each grid cell of the domain has a corresponding value of the latest three parameters. In the case of constant water depths the undisturbed spectrum S_U along the whole domain is equivalent to the incident wave spectrum input at the boundary as there is no transformation due to bathymetry changes. Figure 3 shows the transformation of the wave spectrum for a grid cell located 20 meters on the lee of the device as an example for illustration.

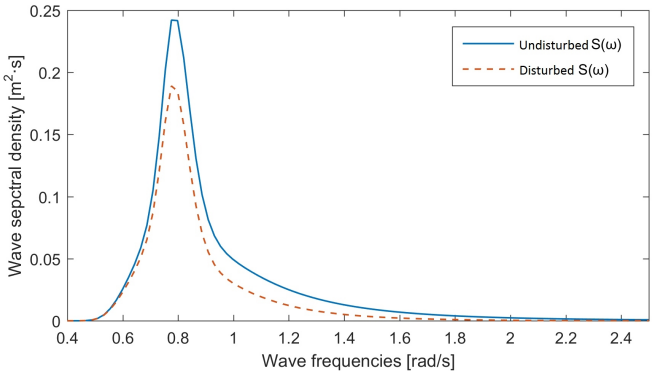

Fig. 3. *Undisturbed wave energy spectrum vs. disturbed wave energy spectrum (behind the WEC).*

The disturbance coefficient K_d defined by equation (15) is then used to quantify with a single parameter the disturbed wave spectrum S_D for each grid cell along the domain. H_{S_D} represents the significant wave height corresponding to the disturbed wave spectrum and H_{S_U} the significant wave height corresponding to the undisturbed wave spectrum.

$$K_d = \frac{H_{S_D}}{H_{S_U}} \tag{15}$$

The calculation of the disturbance coefficient enables the plotting of the wave spectrum changes caused by the perturbation of the WEC along the considered domain. Figure 4 shows the disturbance coefficient K_d obtained along the same domain of 400 x 400 meters for a long-crested irregular sea state with peak period $T_P = 8$ s. Section S, drawn by a dotted line, represents the region where the K_d values are used as a target to tune the absorption coefficients representing the WEC in MILDwave. The disturbance coefficient does not change with the significant wave height of the incident sea state as it is a non-dimensional coefficient and linear waves conditions are assumed. Therefore from now on each sea state is described only by the value of its peak period T_P.

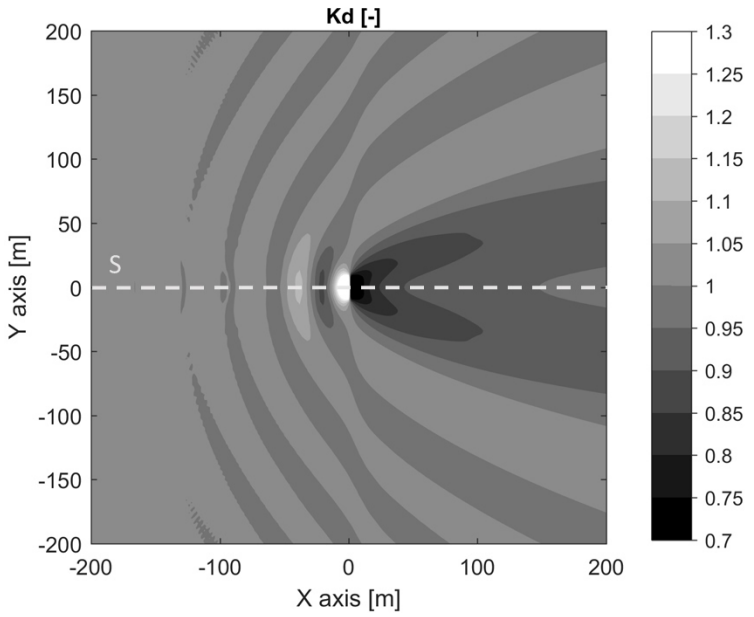

Fig. 4. *Disturbance coefficient from NEMOH for 1 flap and $T_P = 8$ s.*

3.4. Representation in MILDwave

Irregular long-crested waves are generated in MILDwave for the same sea state of $T_P = 8$ s and same domain size as done in NEMOH. The absorption coefficients attributed to the obstacle cells representing the flap type WEC in MILDwave are tuned in such a way that the wave field surrounding the device matches the results obtained from NEMOH.

The flap is represented by a group of grid cells occupying the length of the flap and a thickness of 2 grid cells. A grid cell size of 2 x 2 meters is defined for the cases run in this study. The grid cell size has been chosen to obtain consistent results for all the different sea states considered based on the guidelines from [15]. Different combinations of absorption coefficients were assigned to the

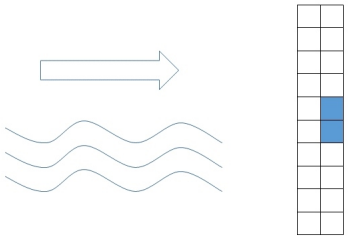

Fig. 5. *Grid cell discretisation of the flap type WEC.*

obstacle grid cells to study the effect on the wave reflection and transmission as part of a sensitivity analysis. The aim of this is to achieve the target disturbance coefficient values to properly represent the flap. Figure 5 shows a sketch of the device grid discretisation where the empty grid cells have the absorption coefficient a set to 0 (fully reflective obstacle) and the coloured grid cells have absorption coefficients a set to a value different than 0 (energy absorbing obstacle).

Table 2 Absorption coefficients configurations

	Absorption coefficient a
Config. 1	0.2
Config. 2	0.3
Config. 3	0.4
Config. 4	0.5

Different values of absorption coefficients are attributed to the coloured cells in order to achieve the target disturbance coefficient distribution along section S. Figure 6 shows the K_d values obtained along section S from MILDwave for the different configurations displayed in table 2 together with the target K_d values from the NEMOH wave solutions.

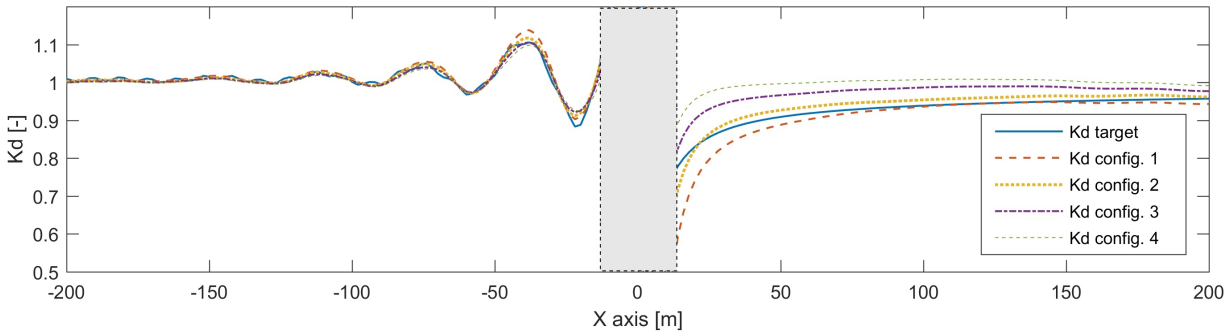

Fig. 6. *Tuning of the absorption coefficients attributed to the WEC grid cells.*

The results obtained for the optimum configuration are shown in the upper plot of Figure 7 where the K_d values along the whole domain are displayed. Configuration 2 has been selected as the one most accurately representing the flap wave disturbance on the wave field for this sea state. The lower plot from Figure 7 shows the percent error between the optimum values obtained in MILDwave and the target values from NEMOH as a comparison plot. The error is relatively large in the near-field but gets reduced extremely fast with the distance to the device. At a radius

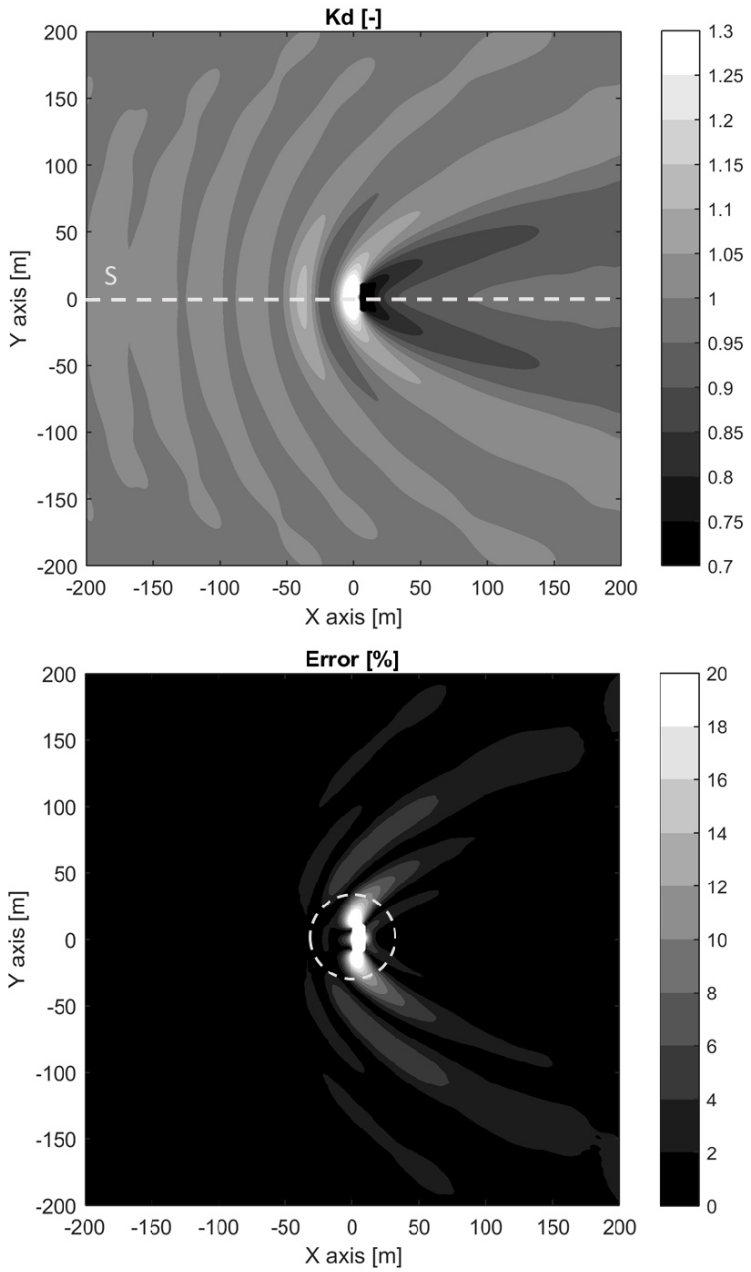

Fig. 7. *Top: Disturbance coefficient from MILDwave for 1 flap and $T_P = 8$ s. Bottom: Percent error between MILDwave and NEMOH (fig. 4) for the same scenario conditions.*

distance higher than 30 meters from the centre of the device (circular dotted line) the error is lower than 10 % and after 50 meters it remains lower than 5%. Thus, the results obtained from modelling the device in MILDwave as a set of obstacle cells show to be representative of the effect of a flap type WEC on the surrounding wave field.

4. Wake effect for a flap type wave energy converter farm

The wake effect for WEC farms composed of several flaps is assessed in this section using MILD-wave. A large domain of 2000 x 1000 m is considered and the wake effect is evaluated in the lee of the farm with a focus on the far-field.

4.1. Wave energy converter farm with 4 flaps

A farm of 4 flaps arranged in a line is first considered. The devices are arranged in a row with a separating distance of 3 x L. The row of flaps is located along section $x = -500$ m allowing the disturbance coefficient K_d to be determined along a length of 1500 meters behind the farm. Figure 8 shows the K_d values obtained for a sea state of $T_P = 8$ s.

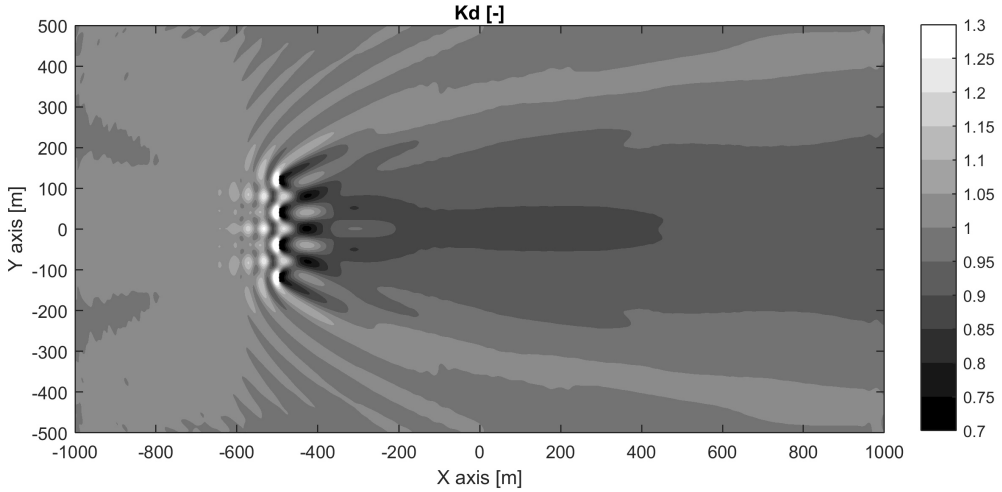

Fig. 8. *Disturbance coefficient for a 4 flaps farm and $T_P = 8$ s.*

Contour lines are plotted in figure 8 along the zones with same K_d values. The darker is the colour of the area with uniform colour the lower is the value of the disturbance coefficient and therefore the higher is the reduction of the significant wave height. The reduction of the disturbance coefficient remain relatively low for this case scenario with only 4 flaps. The area with K_d values ranged between 0.85 and 0.9 (10-15% of significant wave height reduction) is relatively small and the lee side of the farm is dominated by values ranged between 0.9 and 0.95, which corresponds to a 5-10% of significant wave height reduction.

4.2. Wave energy converter farm with 9 flaps

The next step was to model a farm of 9 flaps by adding a second row of 5 devices to the previous setup. The second row is located 20 meters behind the first row (with respect to the incoming waves) and the flaps of the second row are centred about the gaps between the flaps of the first row, as it can be intuit from Figure 9 where the results for this case are shown. The distance in between devices from the second row remain 3 x L as for the first row. This keeps a minimum separating distance of 30 meters (1.5 L) between the devices from the first and second row due to their misalignment.

The location of the second row has been chosen based on the results from the single row case where the disturbance coefficient K_d is higher and therefore the wave energy density is higher as

well. The values of K_d change depending on the location along the domain and the interaction effects of the whole array. Therefore, the locations where a constructive effect on the wave field take place and the disturbed significant wave height increases, are suitable to locate the devices in a attempt to increase the size of the farm. Those spots are exposed to a higher energy density and therefore the WEC is able to extract a higher amount of wave energy. This phenomena is sea state dependent, therefore the devices location needs to be chosen accordingly with the sea state of the site with the highest occurrence probability. The sea state of $T_P = 8$ s is assumed to be the sea state with the highest occurrence probability for this study.

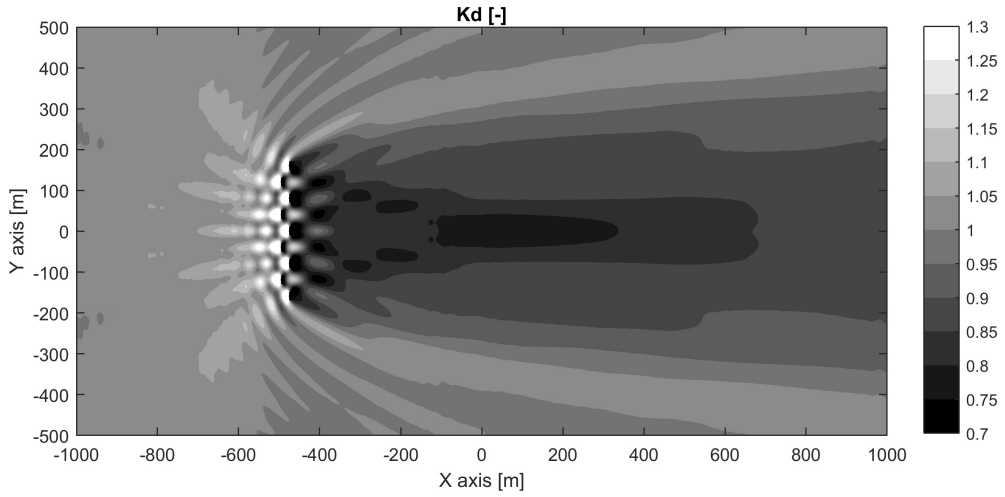

Fig. 9. *Disturbance coefficient for a 9 flaps farm and $T_P = 8$ s.*

As expected, there is significantly lower energy reduction for the 4 flaps farm than for the 9 flaps farm. The higher wave energy absorption and reflection due to the addition of the second row of flaps makes a significant difference in the wake effect. The lowest K_d value obtained for the 4 flaps farm is 0.85 while the equivalent lowest value for the 9 flaps farm is 0.77 considering the fast dissipated near-field results (less than 100 m from the farm) are neglected.

4.3. Farm layout influence

Now, the influence of the separating distance in between devices is assessed. The changes in the separating distance leads to important changes in the wake effect due to the amount of wave energy density passing between the flaps. A separating distance of $3L$ was used in the previous case studies and now two additional configurations with a separating distance of 4 and 5 times L are considered. The same distance of 20 m between rows is kept and the flaps of the second row are centred in the gaps from the front row. A sea state of $T_P = 8$ s is applied in this section.

Figure 10 show the disturbance coefficient obtained for the $4L$ and $5L$ cases respectively and can be compared with the results from Figure 9 where a separating distance of $3L$ was considered under the same incident wave conditions.

It can be seen that the higher reduction of the disturbance coefficient is not achieved with the shortest separating distance of $3L$ as one could logically think but with a separating distance of $4L$. A large area corresponding to the Kd values below 0.75 (equivalent to a 25% of significant wave height reduction) is found for the $4L$ case while a much smaller area corresponding to the same values is found for the $3L$ and $5L$ cases. Therefore the highest sheltering effect is found for

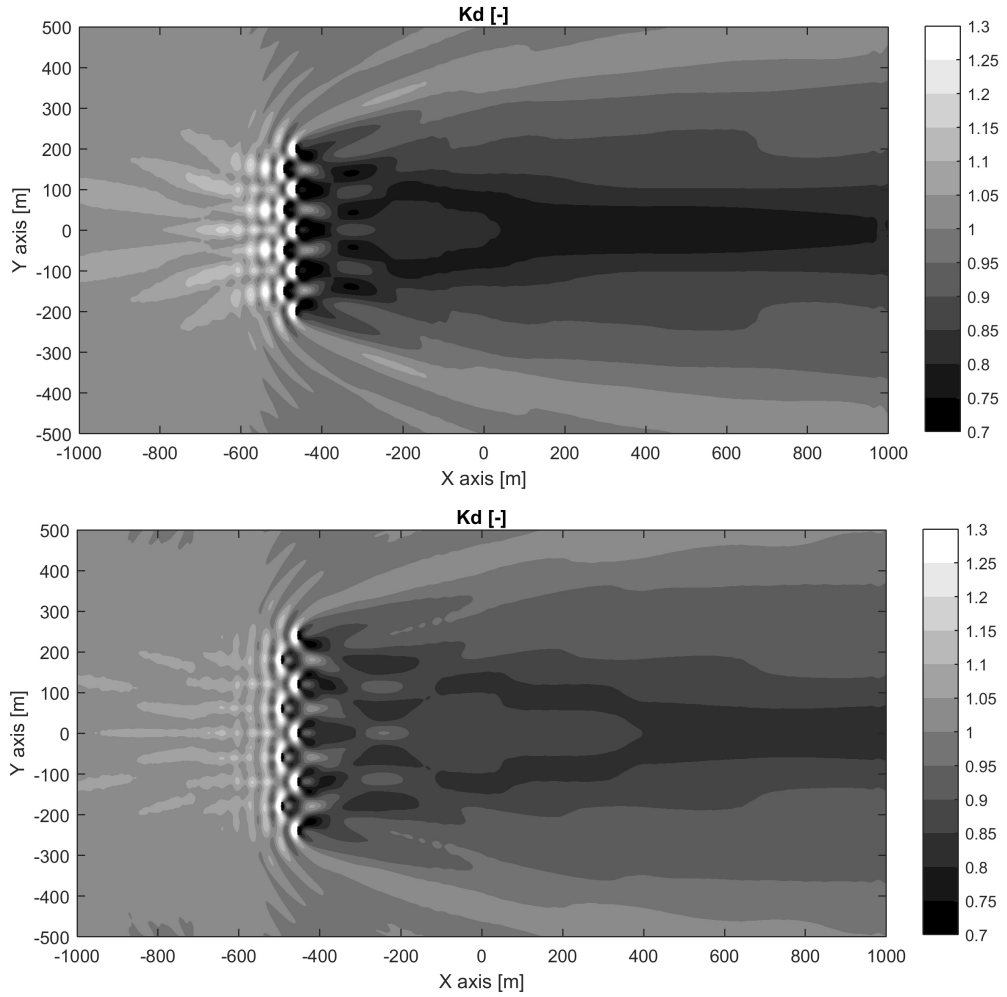

Fig. 10. *Disturbance coefficient for a 9 flaps farm and $T_P = 8$ s. Top: Spacing in between devices of 4 L. Bottom: Spacing in between devices of 5 L.*

the $4L$ case as is the configuration under which the highest reduction of energy density is found. Nevertheless a similar area size is found for the 3 cases (3, 4, and 5 L) if the zone corresponding to the K_d values below 0.9 is considered, which represents only a reduction of 10% in the significant wave height.

From now on, the $3L$ configuration of the 9 flaps farm will be used to assess the influence of the sea state and batheymetry on the wake effect.

4.4. Sea state influence

The influence of the sea state in the wake effect is now assessed in this section. A farm composed of two rows and 9 flaps with the same configuration than the last section is considered. Two sea states of $T_P = 6$ s and then a $T_P = 10$ s are considered. The tuning of the absorption coefficients attributed to the obstacle cells representing the flaps has been done again for every sea state. Therefore an optimum configuration of the device representation has been obtained for every sea state.

Figure 11 shows the disturbance coefficient obtained for the sea state $T_P = 6$ s and $T_P = 10$ s.

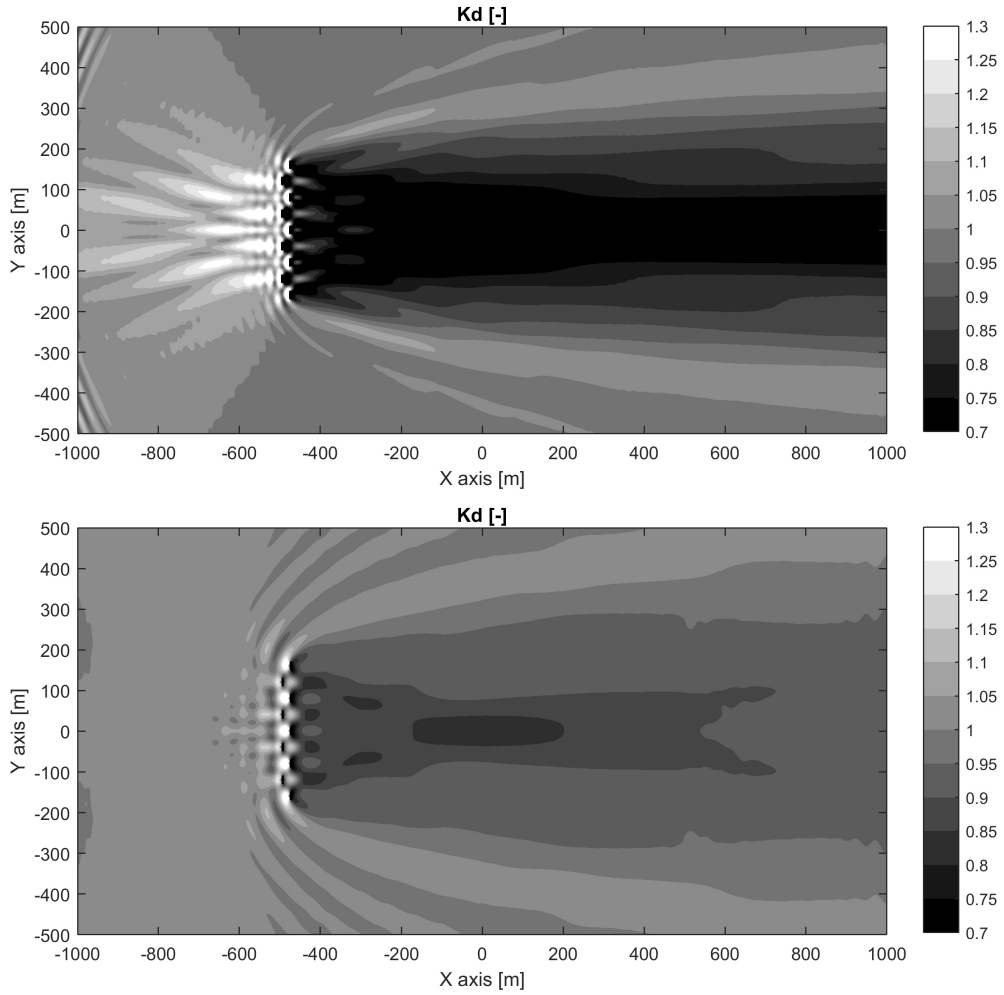

Fig. 11. *Disturbance coefficient for a 9 flaps farm. Top: sea state of $T_P = 6$ s. Bottom: sea state of $T_P = 10$ s.*

A large decrease in the disturbance coefficient is found for the first sea state while no significant difference is found for the second sea state. The reason for such a high disturbance of the farm under the sea state of $T_P = 6$ s is the ratio between the wave length corresponding to the peak period and length of the flaps. The diffraction phenomena becomes significant for ratios between obstacle characteristic length and wave length larger than 0.2 [13]. In this case the characteristic length of the device is 20 meters and the wave length for the peak period is about 50 meters, therefore diffraction effects are important and lead to a much higher wave field disturbance than for the case of $T_P = 8$ s and $T_P = 10$ s.

5. Changing depth bathymetry influence

When waves propagate from deep to shallow water shoal will occur and the wave height will increase while the waves travel towards decreasing depths. In this section the influence of a changing depth bathymetry on the wake effect of a flap farm is investigated. Then a comparison is made with the constant water depths scenario considering the same farm configuration and sea state. This is

done as a step in enhancing the use of this method to real scenarios where there would be a variable bathymetry.

The bathymetry is represented by a constant depth profile along the Y axis and a changing depth profile with a mild-slope along the X axis. A sketch representation of the mild-slope profile is shown in figure 12. The slope starts at $x = 500$ with 10 meters of water depth and finishes at $x = 0$ with 5 meters of water depth. A dotted line has been drawn on top of next results from figure 13 in order to represent the section along the domain corresponding to the profile.

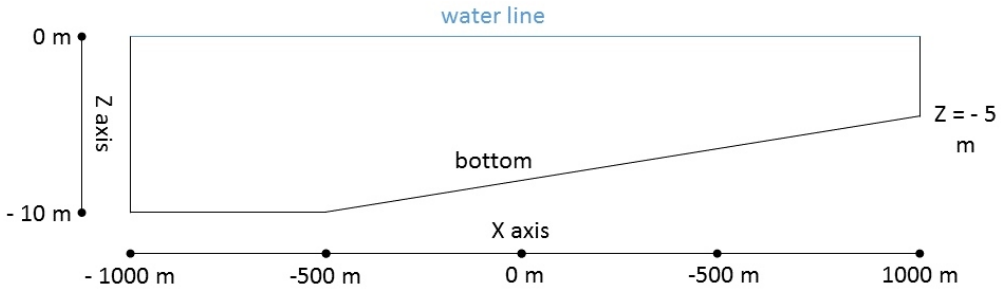

Fig. 12. *Bathymetry profile along X axis.*

First the waves are propagated throughout an empty domain (absence of WEC farm) where the significant wave height get transformed with the shoaling effect. The local significant wave height obtained at each grid cell along the empty domain is then used as the undisturbed significant wave height from the dividing term of the disturbance coefficient shown in equation (15). Results of the obtained K_d values are shown in figure 13 for a state of $T_P = 8$ s.

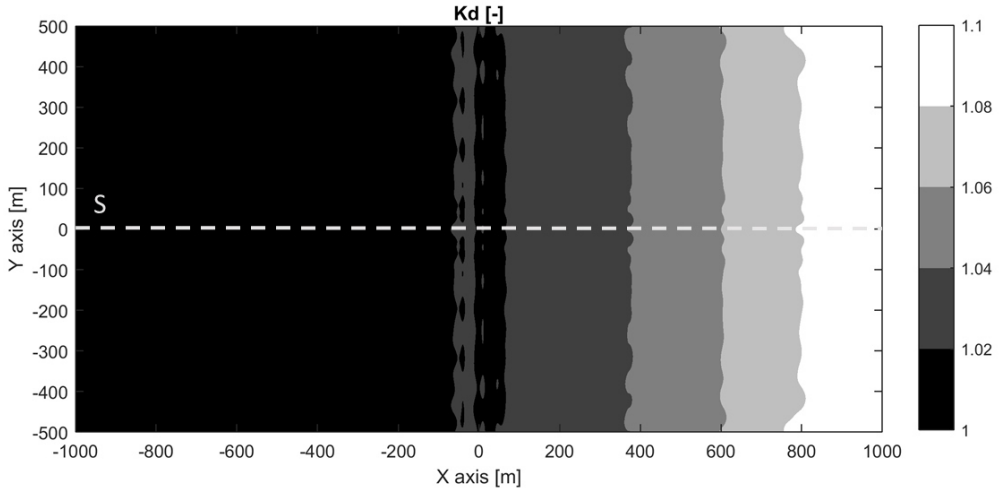

Fig. 13. *Disturbance coefficient for an empty domain with a mild-slope bathymetry and $T_P = 8$ s.*

Now the farm of 9 flaps is modelled and the waves are propagated throughout the domain with the same bathymetry profile from figure 12. The undisturbed significant wave height used to obtain disturbance coefficient K_d locally for each grid cell is obtained in this case from the significant wave height corresponding to the empty domain case. Thus, when a changing depth bathymetry is considered, an empty domain case needs to be computed first to assess the significant wave height in the absence of WECs in order to evaluate correctly the wake effect of the WEC farm.

The upper plot of figure 14 shows the disturbance coefficient obtained for the same sea state as the empty domain case. The lower plot shows the percent difference between the K_d values obtained with the mild-slope bathymetry and the case with a constant depth from figure 9. The output shows good similarity in terms of the disturbance coefficient areas with the same sheltering provided for both constant water depths or changing bathymetries. The percent difference plot shows that the maximum difference obtained remains bellow 3%, which is a negligible quantity. Therefore, based on this first approach the sheltering effect provided by a flap type WEC farm does not seem to be largely influenced by bathymetries with mild-slopes where the depth decreases progressively towards the wave propagation direction.

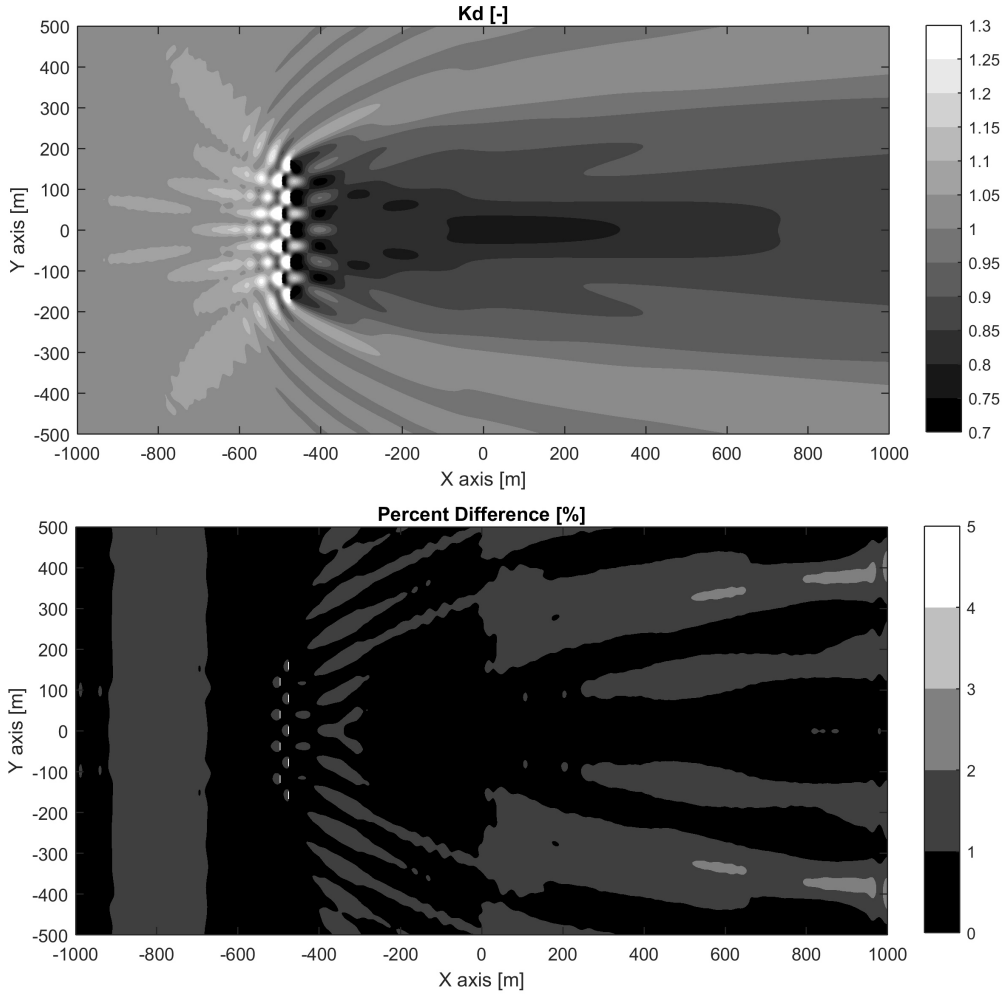

Fig. 14. *9 flaps farm and mild-slope bathymetry scenario for a $T_P = 8$ s. Top: Disturbance coefficient. Bottom: Percent difference with constant water depth case from fig. 9.*

6. Discussion

The technique employed to represent a wave energy converter in a mild-slope equation model has shown to give an accurate representation of the wave field perturbation generated by a single device. The technique has been verified using output from NEMOH which has shown that the error

reduces quickly as the distance from the device increases. Interaction effects between devices can play an important role for cases where the WECs are closely spaced and located at a distance in between themselves shorter than the error dissipation. In this case, a solution can be to represent the multiple device in NEMOH in order to account for the devices interactions in the target wave field, noting that this can be a computational time demanding task. The potential influence of the devices interactions was neglected in this study as a large enough separating distance has been left for the cases considered. However, a validation scenario where a farm of various WECs is modelled in NEMOH and compared against results from MILDwave would allow to define with more precision the minimum distance to leave until interaction effects are completely dissipated.

Following the validation of the single WEC modelling, wake effects of WEC farms were assessed for different scenarios changing the incident sea state conditions, the farm layout configuration, and the bathymetry. The results shown first that adding a second row of devices to a single row farm by blocking the gaps in between devices from the first row leads to a larger sheltered area and to a higher significant wave height reduction in the lee of the farm. It is worthwhile to deploy the farms of flap type WECs following a scheme of two rows as it has been shown that the sheltering effect is increased and the devices from the second row can be exposed to higher energy density locations. In addition to this, deploying closely spaced devices in a farm allow for cabling cost reductions.

The influence between the wake effect and the distance separating the devices was proven with the largest reduction of the wave energy density found for the $4L$ spacing distance. The interaction of the individual wake effects of each device in the lee of the farm lead to a higher decrease of the minimum significant wave height values for a specific area. However, if the results are compared with a broader perspective, the areas with K_d values remaining under 0.9 (minimum of a 10 % significant wave height reduction) remain really similar.

The wake effect variability due to the incident sea state for the same farm configuration has been shown to be the most influencing variable. A large reduction of the significant wave height is found for the $T_P = 6$ s compared to the $T_P = 8$ s and $T_P = 10$ s. The lowest K_d value obtained for the $T_P = 6$ s case along the large area of reduction is 0.62. The large difference between those cases is due to the diffraction phenomena becoming significant for small wave periods, due to the ratio between the wave length of the peak period and the flap length. The sheltered area changes significantly depending of which K_d value is set as the maximum value guaranteed in the area. Large sheltered areas are found for all sea states if a maximum $K_d = 0.9$ (minimum of a 10 % significant wave height reduction) is set as the limit whereas, if the maximum limit is set to $K_d = 0.7$ (minimum of a 30 % of significant wave height reduction), only sea states of $T_P = 6$ s can provide large sheltered areas.

Finally, the influence of the changing depth was assessed and it was found that for a progressively changing depth with a mild-slope the wake effect remains similar. The maximum difference with the constant water depth case was lower than 3%. It is important to notice that no dissipative processes such as wave breaking were applied. Approaching the end of the domain (right hand side) at the shallow water location the wake effect will probably be significantly influenced by wave breaking and this would lead to a higher reduction of the significant wave height at that location and therefore, to a higher difference with the constant water depth case. In addition, a real bathymetry where depth changes irregularly across both X and Y direction will lead do irregular variations in the undisturbed significant wave height along the domain and thus to a different shape of the wake effect.

7. Conclusion

It was found that changes in the layout of the WEC farm can lead to much larger significant wave height reductions on the lee side, particularly the distribution of the farm in two rows of WECs. By adapting the layout configuration of the farm to the sea state with the highest occurrence at the deployment location, notable improvements in the significant wave height reduction can be obtained. Achieving large sheltered areas in the immediate vicinity of the WECs, can benefit other marine activities such as offshore wind and aquaculture. For instance, offshore wind farms O&M weather windows can be increased and risks associated with turbines access can be reduced. Already the Floating Power Plant platform has demonstrated the benefit of reduced wave conditions on the lee side for operational activities. Aquaculture farms can benefit from a reduction on the hydrodynamic loads on the structures and increase the weather windows for the feeding activities. The method can effectively demonstrate the far field effects of a WEC array which is of particular concern at sites where there is surfing activity or when the farm is being located in a sensitive environmental area.

Finally as an overall conclusion, the methodology has demonstrated an improvement on the modelling techniques to represent WECs in wave propagation models. The accuracy of the target device reflection and transmission used to tuned its representation in the wave propagation model has been improved compared to previous studies. A 2D representation of the wave field disturbance generated by a WEC has been used as a target information compared to the usual 1D wave field disturbance information from previous studies. In addition, the results have been validated against the target results with comparison plots for the near-field. Therefore, the methodology can represent realistic scenarios with WEC farms deployed at locations with irregular bathymetries where important wave transformation processes such as refraction, shoaling, reflection, transmission and diffraction intrinsically, occur.

8. Acknowledgment

The research leading to these results is part of the OceaNET project, which has received funding from the European Union's Seventh Framework Programme for research, technological development and demonstration under grant agreement no 607656.

9. References

9.1. Journal articles

[1] Borgarino, B., Babarit, a., Ferrant, P.: Impact of wave interactions effects on energy absorption in large arrays of wave energy converters, Ocean Eng., 2012, 41, pp. 79-88.

[2] Mcnatt, J.C., Venugopal, V., Forehand, D.: A novel method for deriving the diffraction transfer matrix and its application to multi-body interactions in water waves, Ocean Eng., 2014, 94, pp. 173-185.

[3] Smith, H.C.M., Pearce, C., Millar, D.L.: Further analysis of change in nearshore wave climate due to an offshore wave farm: An enhanced case study for the Wave Hub site, Renew. Energy, 2012, 40, (1), pp. 51-64.

[4] Astariz, S., Abanades, J., Perez-Collazo, C., Iglesias, G.: Improving wind farm accessibility for operation & maintenance through a co-located wave farm: Influence of layout and wave climate, Energy Convers. Manag., 2015, 95, pp. 229-241.

[5] Beels, C., Troch, P., De Backer, G., Vantorre, M., De Rouck, J.: Numerical implementation and sensitivity analysis of a wave energy converter in a time-dependent mild-slope equation model, Coast. Eng., 2010, 57, (5), pp. 471-492.

[6] Beels, C., Troch, P., De Visch, K., Kofoed, J.P., De Backer, G.: Application of the time-dependent mild-slope equations for the simulation of wake effects in the lee of a farm of Wave Dragon wave energy converters, Renew. Energy, 2010, 35, (8), pp. 1644-1661.

[7] Radder, A.C., Dingemans, M.W.: Canonical equations gravity waves, weakly nonlinear gravity waves, Wave Motion, 1985, 7, pp. 473-485.

[8] Lee, C., Suh, K.D.: Internal generation of waves for time-dependent mild-slope equations, Coast. Eng., 1998, 34, (12), pp. 35-57.

[9] Lee, C., Kim, G., Suh, K.D.: Extended mild-slope equation for random waves, Coast. Eng., 2003, 48, (4), pp. 277-287.

[10] Zhao, H. tao, Sun, Z. lin, Hao, C. ling, Shen, J. fa: Numerical modelling on hydrodynamic performance of a bottom-hinged flap wave energy converter, China Ocean Eng., 2013, 27, (1), pp. 73-86.

9.2. Conference Paper

[11] Folley, M., Babarit, A., Child, B., et al.: A Review of Numerical Modelling of Wave Energy Converter Arrays, in Proc. 31st Int.Conf. on Ocean, Offshore and Arctic Engineering, Rio de Janeiro, Brazil, July 2012, pp. 535-545

[12] Babarit, A., Delhommeau, G.: Theoretical and numerical aspects of the open source BEM solver NEMOH, Proc. 11th Eur. Wave Tidal Energy Conf., 2015, pp. 1–12.

9.3. Book

[13] Sarpkaya, T., Isaacson, M.: 'Mechanics of wave forces on offshore structures', Van Nostrand Reinhold Co., 1981.

[14] Troch, P., Stratigaki, V.: 'Phase-resolving wave propagation array models', in 'M. Foley (Ed.), Numerical modelling of wave energy converters: state-of-the-art techniques for single devices and arrays', Elsevier, 2016, pp. 191-216.

9.4. Report

[15] Troch, P. 1998. MILDwave A numerical model for propagation and transformation of linear water waves, Internal Report, Department of Civil Engineering, Ghent University.